Catalysis Today 181 (2012) 124–132

Contents lists available at ScienceDirect

Catalysis Today

journal homepage: www.elsevier.com/locate/cattod

Water interaction with CeO_2(1 1 1)/Cu(1 1 1) model catalyst surface

V. Matolín[a,*], I. Matolínová[a], F. Dvořák[a], V. Johánek[a], J. Mysliveček[a], K.C. Prince[b,c], T. Skála[b], O. Stetsovych[a], N. Tsud[a], M. Václavů[a], B. Šmíd[a]

[a] Charles University, Faculty of Mathematics and Physics, Department of Surface and Plasma Science, V Holešovičkách 2, 18000 Prague 8, Czech Republic
[b] Sincrotrone Trieste, Strada Statale 14, km 163.5, 34149 Basovizza-Trieste, Italy
[c] TASC Laboratory, IOM-CNR, Strada Statale 14, km 163.5, 34149 Basovizza-Trieste, Italy

ARTICLE INFO

Article history:
Received 16 March 2011
Received in revised form 19 May 2011
Accepted 30 May 2011
Available online 25 June 2011

Keywords:
Cerium oxide
Water adsorption
Hydroxyl
Photoelectron spectroscopy
STM
TPD

ABSTRACT

Interaction of water with fully oxidized and partially reduced CeO_2(1 1 1) thin film model catalyst grown on a Cu(1 1 1) surface was investigated by photoelectron spectroscopy (PES), scanning tunneling microscopy (STM) and temperature programmed desorption (TPD). On the stoichiometric surface water adsorbs molecularly at low temperatures ($\leq$120 K) while on the reduced surface the adsorption is partially dissociative with formation of OH groups. STM indicates no morphology variation and a very sensitive Ce 4d–4f resonant photoelectron spectroscopy (RPES) no noticeable change of the oxidation state of ceria upon water adsorption and subsequent complete desorption. Formation of co-adsorbed phase of residual water with OH during molecular water desorption, on the other hand, leads to a substantial resonance of the Ce^{3+} photoemission state around 170 K. We propose that this behaviour indicating ceria reduction is in this case an electronic effect of the Ce 4f charge accumulation and Ce 5d charge depletion.

1. Introduction

Many studies were devoted to the water molecule study in the past because water is essential for all life processes [1] as well as for many catalytic processes, e.g. for water-gas-shift (WGS) reaction. Photoelectron spectroscopy is a powerful method of investigation of electronic structure of molecules. Winter et al. [2] used valence band photoelectron spectra of liquid water to analyze its electronic structure and found that it was similar to that of ice. Chemical bonding of water to metal surfaces was studied using core level X-ray photoelectron spectroscopy (XPS) in [3–5] presenting an understanding of water adsorption process by combining XPS results with first principle calculations [4,5]. Ambient pressure XPS provided on metals and oxides [6] confirmed that a general trend in water adsorption is an initial formation of hydroxyl group followed by molecular water adsorption. Adsorption of water on CeO_x(1 1 1) grown on Ru(0 0 0 1) was investigated in [7]. It was shown that water adsorbed in molecular form on stoichiometric CeO_2(1 1 1) while on reduced cerium oxide surfaces hydroxyls were detected in addition to molecular water. Watkins et al. [8] investigated the process of water adsorption using DFT calculations suggesting that for the stoichiometric surface water molecule dissociates into an OH group bonded to cerium and an H atom bonded to a surface oxygen atom. For the case of the reduced surface, the same authors found that the OH group produced by the water dissociation fills the oxygen vacancy while the H atom bonds to a surface oxygen atom. On the contrary, Fronzi at al. [9] found by DFT that clean CeO_2(1 1 1) surface does not dissociate water and that water dissociation is favored only on a reduced surface in agreement with experimental observations [7]. This substantial difference between the fully oxidized and the reduced ceria surfaces stresses the importance of oxygen vacancies for water dissociation on this system.

WGS reaction was also investigated on an inverse model CeO_x/Au(1 1 1) catalyst in [10]. The experiment confirmed that water molecules dissociate readily in the presence of Ce^{3+} and form hydroxyls remaining at the surface up to 600 K.

In order to experimentally verify the mechanism of water ceria interaction, we used a thin film CeO_2 model catalyst prepared under ultrahigh-vacuum conditions by reactive growth on a Cu(1 1 1) substrate [11,12]. Oriented thin films of ceria CeO_2(1 1 1) on Cu(1 1 1) [11–13] became important model systems in the research of catalysis over ceria. Chemical reactivity of ceria on Cu(1 1 1) was investigated for discontinuous layers (inverse model catalysts) [14–17], continuous layers [18,19], as well as continuous layers activated with deposited metal clusters [20–22]. Morphology of the CeO_2 thin films in our study was characterized by scanning tunneling microscopy (STM) that typically reveals oriented CeO_2(1 1 1) terraces separated by monolayer-high steps [19,23].

* Corresponding author.
E-mail address: matolin@mbox.troja.mff.cuni.cz (V. Matolín).

0920-5861/$ – see front matter © 2011 Elsevier B.V. All rights reserved.
doi:10.1016/j.cattod.2011.05.032

The conventional experimental approach to water–ceria interactions relies on the analysis of Ce and O core level spectra and valence band spectra. However, the effects related to the interactions are minute and, therefore, difficult to identify. In this study, we use resonant photoelectron spectroscopy (RPES) (see [24,25] and references therein), which is probably the most sensitive surface science tool to follow changes in the oxidation state of ceria. Briefly, the method exploits the selective resonant excitations 4d–4f in Ce^{3+} ($4d^{10}4f^{1}$) and Ce^{4+} ($4d^{10}4f^{0}$). The excited states decay via Super-Coster-Kronig processes, leading to a strong enhancement of certain valence band features. For Ce^{3+}, the resonance gives rise to a feature at 1.7 eV binding energy (BE), with a maximum enhancement at photon energy (PE) of 121.5 eV, whereas for Ce^{4+}, the feature appears at 4 eV BE with the maximum enhancement at 124.8 eV PE.

2. Experimental

The photoelectron spectroscopy measurements have been performed at the Materials Science Beamline of the synchrotron light source ELETTRA in Trieste, Italy. The photoemission spectra were acquired using a high luminosity electron energy analyzer (Specs Phoibos 150) with 150 mm mean radius, equipped with a 9-channel detector. The experimental end station was equipped with a rear view LEED optic, a quadrupole mass spectrometer, an argon sputter gun, and a gas inlet system. The spectra were normalized with respect to the ring current. The resonant photoelectron spectra were recorded at variable excitation energies between 115 and 124.8 eV in order to detect the Ce 4f valence band states. The resonant photoelectron spectra of Ce 4f states yield highly-resolved information about concentration of Ce^{3+} ions in the ceria surface in the form of the so-called resonant enhancement ratio (RER) = $D(Ce^{3+})/D(Ce^{4+})$ [24]. This parameter is defined as the ratio of the resonant enhancements of on- and off-resonance feature intensities related to Ce^{3+} [$D(Ce^{3+})$, on-resonance at PE = 121.4 eV, off-resonance at PE = 115.0 eV] and Ce^{4+} [$D(Ce^{4+})$ on-resonance at PE = 124.8 eV, off-resonance at PE = 115.0 eV]. Ce 3d, O 1s, and C 1s core level spectra were measured using Al Kα radiation. The XPS Ce 3d and O 1s spectra were taken at 20° and 60° photoelectron emission angles (with respect to the surface normal), respectively, in order to detect both signals from comparable depths. Cerium (Goodfellow, 99.99%) was evaporated at a constant deposition rate using an electron-beam evaporator with a Mo crucible onto the clean Cu(1 1 1) substrate at 523 K in an oxygen atmosphere of 5×10^{-7} mbar, followed by annealing under identical conditions for 10 min. The deposition rate was 0.08 ML min^{-1}, as calibrated by means of a quantitative analysis of the Cu 2p intensity. Here we define 1 monolayer (ML) of ceria as corresponding to a O–Ce–O trilayer of the CeO_2(1 1 1) fluorite bulk structure, with a thickness of 3.13 Å. Water was introduced into the chamber by a leak valve at the pressure of 6.6×10^{-7} mbar for 200 s, giving a total exposure of 100 L.

In order to compare water adsorption on stoichiometric and partially reduced ceria surfaces we created reduced CeO_{2-x}/Cu(1 1 1) samples artificially by Ar^+ sputtering of the surface (1 keV ion energy, 12 μA/cm^2 ion current density, 1 min) followed by a mild 2-min annealing at the temperature equal to that during ceria layer growth (523 K).

STM measurements were performed in another chamber on a homemade STM system with 1×10^{-10} mbar base pressure. Cu(1 1 1) substrates were cleaned by repeated Ar^+ sputtering and annealing in vacuum. CeO_2 was grown by evaporation of Ce in 5×10^{-7} mbar of oxygen. Ce was evaporated using an identical evaporator as the one at Elettra. The coverage of CeO_2 was determined using quartz crystal microbalance. STM images of the morphology of ceria films were acquired with chemically etched tungsten tips at room temperature. TPD was measured by means of a quadrupole mass spectrometer placed in a differentially pumped nozzle (to eliminate background contribution during thermal desorption) installed in the same vacuum system. The sample heating rate during TPD was set to 2 K/s.

3. Results and discussion

3.1. STM study

We used STM to characterize and compare morphologies of both 10 ML-thick ceria layers on Cu(1 1 1) investigated in the present study: a stoichiometric CeO_2 oxide, and reduced CeO_{2-x} prepared by Ar^+ sputtering. We obtain images both before and after interaction of samples with water. We complement the information on morphology of the layers with highly sensitive measurements of Ce^{3+} concentrations in the layers using RER DCe^{3+}/DCe^{4+} (cf. Ref. [23]).

Surface morphology of the stoichiometric CeO_2 layer on Cu(1 1 1) is shown in Fig. 1a. The surface of the layer comprises oriented CeO_2(1 1 1) terraces separated by monolayer-high steps. Characteristic length of a terrace is about 10 nm. The step height of 0.31 nm corresponds to the spacing of the O–Ce–O trilayers in CeO_2(1 1 1) bulk single crystal. We observe 3–4 open ceria monolayers organized in broad pyramids (cf. [23]). In Ref. [23] it was shown that the majority of the residual Ce^{3+} in the stoichiometric layers is located at step edges. An undercoordinated step edge site thus seems to be a characteristic defect of the stoichiometric layer. In the present experiment, measured DCe^{3+}/DCe^{4+} after cooling the samples down to 120 K was less than 0.15 depending on the residual water pressure.

Morphology of the reduced CeO_{2-x} surface after 3 min irradiation with 1 keV Ar^+ ions, 2 μA/cm^2 (total ion dose equivalent to that used in PES/XPS experiment), and subsequent 2 min annealing to 523 K in vacuum is shown in Fig. 1b. It can be noticed that the CeO_2(1 1 1) terraces observed in Fig. 1a were disintegrated into small islands with a characteristic diameter less than 5 nm. The layered structure of CeO_2(1 1 1) film seems to have been conserved. We can still see 3–4 open ceria monolayers and monolayer-high steps separating them. We can estimate that the ion bombardment increases the density of step edges and kink sites approximately by a factor of two. On the contrary, DCe^{3+}/DCe^{4+} increases by an order of magnitude to 1.3 on samples at 120 K. The increase of DCe^{3+}/DCe^{4+} upon ion bombardments seems to be substantially higher than what would correspond to the increase of step density in STM images (cf. Ref. [23]). Thus, we must allow for the existence of another type of Ce^{3+} sites, most likely surface oxygen vacancies in the terraces on the sputtered samples.

Both the as-deposited and the Ar^+ sputtered samples were subject to adsorption of H_2O at 100 K and temperature-programmed desorption to 500 K. STM images of the samples after water desorption are shown in Fig. 1c and d. We identify no observable change of island size, step density, or step geometry upon water desorption from stoichiometric CeO_2 layer (cf. Fig. 1a and c), and, given the lower resolution of STM image in Fig. 1d, no observable change of island size or step density in the reduced CeO_{2-x} layer (cf. Fig. 1b and d). More importantly, DCe^{3+}/DCe^{4+} for the stoichiometric CeO_2 layer after adsorption and desorption of water are identical, allowing us to conclude that water adsorption and desorption induces no changes to the morphology and Ce^{3+} content of stoichiometric CeO_2 layers. For reduced CeO_{2-x} layers the morphology remains conserved as well while the DCe^{3+}/DCe^{4+} increases from 1.3 to 1.8 most likely due to uncomplete desorption of water fragments from Ar^+ sputtered CeO_2 at 500 K.

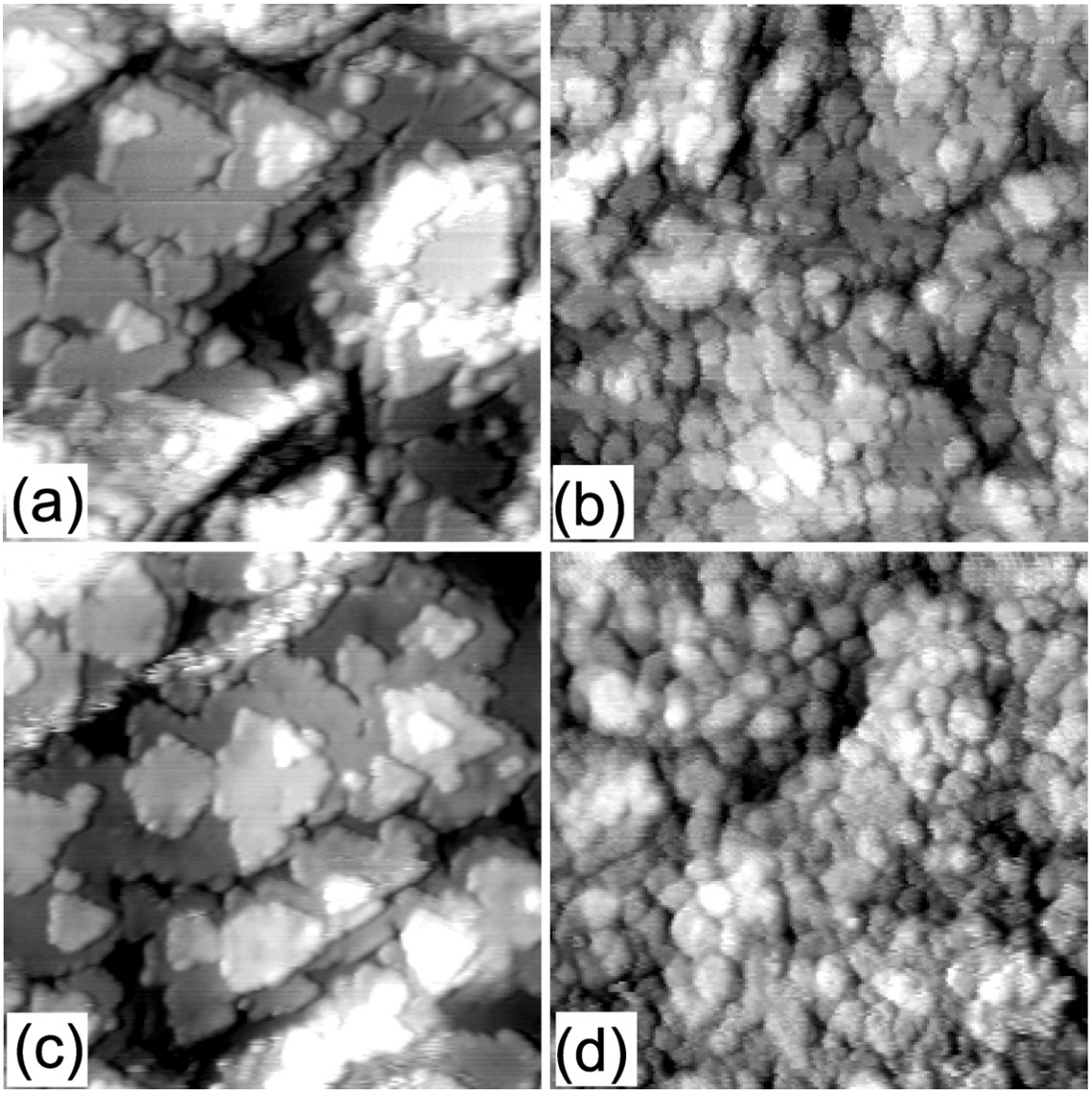

Fig. 1. Morphology of 10 ML-thick ceria layer on Cu(1 1 1) as deposited (a, stoichiometric CeO_2) and after Ar^+ sputtering (b, reduced CeO_{2-x}). The CeO_2(1 1 1) terraces apparent in (a) have disintegrated into small islands with characteristic diameter less than 5 nm in (b). (c and d) Layers as in (a) and (b) after adsorption and desorption of water. STM topographs were obtained at room temperature, image size in (a)–(d) 50 nm × 50 nm.

3.2. Photoelectron spectroscopy and temperature programmed desorption

In Fig. 2 the on-resonance valence band spectra (PE = 121.5, 124.8 eV) obtained for stoichiometric CeO_2 (Fig. 2a) and reduced CeO_{2-x}/Cu(1 1 1) (Fig. 2b) samples $x > 0$ at room temperature are displayed, together with valence band spectra taken off-resonance (PE = 115 eV). The arrows in the figures indicate the on-off resonance enhancements D(Ce^{3+}) and D(Ce^{4+}) used to calculate the resonant enhancement ratio (RER) = D(Ce^{3+})/D(Ce^{4+}) [24]. The RER directly reflects the Ce^{3+}/Ce^{4+} ion ratio in partially reduced CeO_{2-x} and can be calibrated in terms of the nonstoichiometry factor x by comparing to the fitted Ce 3d core level spectra (note that this procedure disregards differences in the electron mean free path for the two methods; see for example Ref. [20]). The results in Fig. 2a show for CeO_2 RER being nearly zero indicating well stoichiometric cerium oxide in the case of the as-prepared sample. In Fig. 2b we observe that Ar^+ sputtering creates a considerably reduced surface (cf. Section 3.1).

In order to identify the variations of the cerium oxidation state due to water–oxide interaction, we measured changes in the on-resonance and off-resonance valence band spectra upon water adsorption at 120 K and during the subsequent annealing. We should note that the substantial intensity of the resonant features determined from the present RPES experiment can be related not only to the generally high sensitivity of RPES but also to the highest surface sensitivity of the present synchrotron-radiation-based experiment working with kinetic energy of emitted electrons around 120 eV. Thus the use of this method is consistent with the assumption that the water interaction initially affects the surface region, i.e. ceria modification is seen in the vicinity of the water molecules and/or their fragments.

The on-resonance and off-resonance spectra obtained upon water adsorption and annealing of the stoichiometric sample (see Fig. 1a) are presented in Fig. 3 together with the spectra of the clean sample. The clean sample spectra were taken at 120 K contrary to those in Fig. 2 obtained at room temperature. By comparing these spectra we can see that cooling of the sample was accompanied by

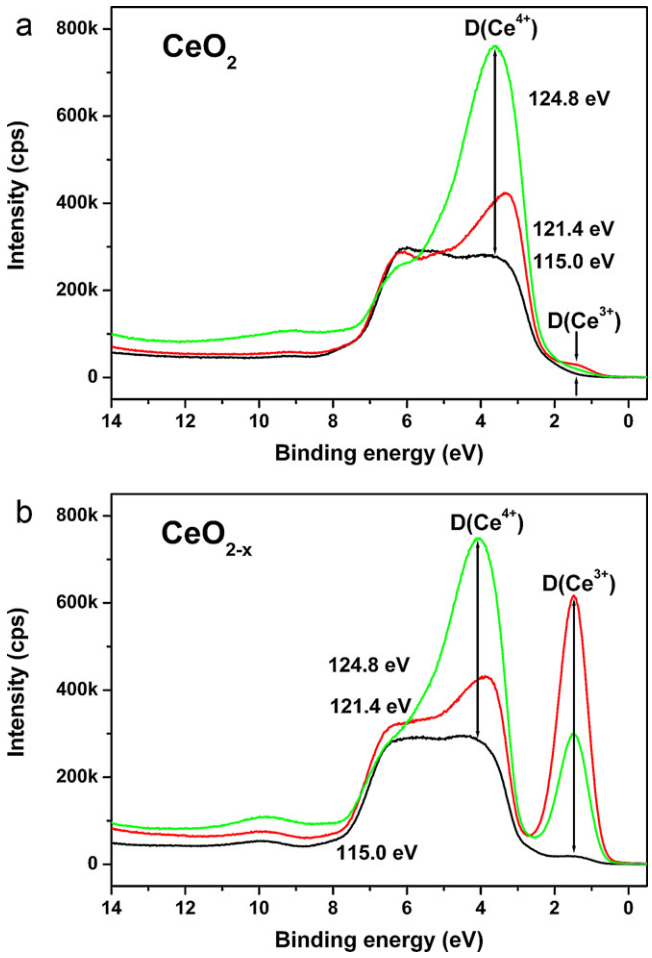

Fig. 2. On- and off-resonance valence band spectra taken at PE = 124.8, 121.4 and 115 eV. Arrows indicate resonance enhancement used for determination of RER. Stoichiometric CeO_2(1 1 1) surface (a) and reduced CeO_{2-x}(1 1 1) surface (b).

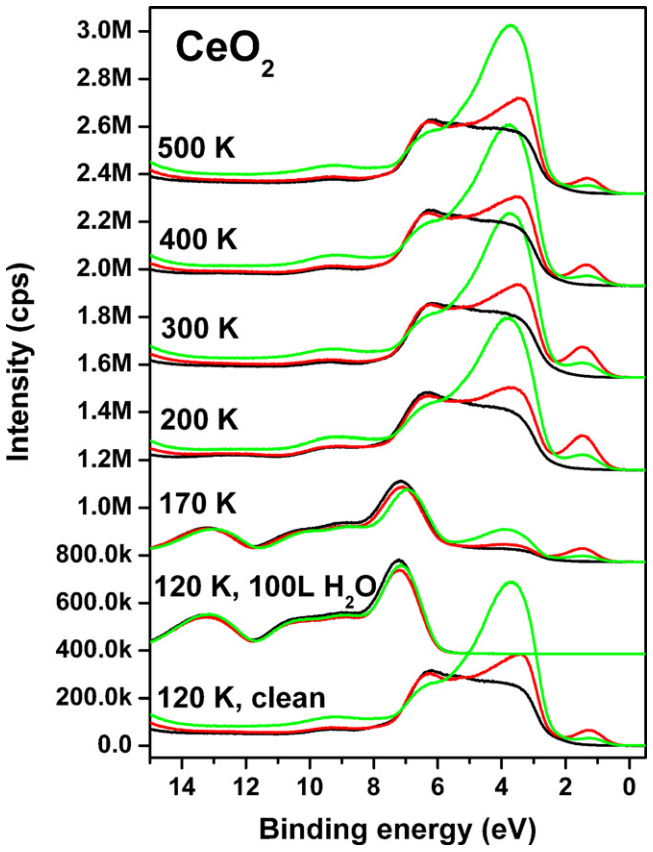

Fig. 3. On- and off-resonance valence band spectra for CeO_2(1 1 1) upon water adsorption and consequent annealing.

appearance of Ce^{3+} resonant states. Subsequent multilayer water adsorption at 120 K completely blocked the photoemission from the ceria substrate due to low photoelectron escape depth. The VB spectrum of water multilayer reveals characteristic molecular features of thick water layer (e.g. [26] on oxide and [27] on metal) and resemble the spectrum of liquid water [2].

Upon annealing to 170 K the spectra show that limited amount of water molecules remain on the surface because water features (BE 6–16 eV) are mixed with VB spectra of cerium oxide. By comparing intensities of the O 2p band (BE 3–7 eV) which dominates the off-resonance spectra we can see that spectra of ceria are strongly attenuated by the adsorbed water. We can estimate from the decrease of the off-resonance O 2p band intensity that the amount of residual water corresponds to approximately 2 ML (assuming an inelastic mean free path of 0.8 nm [28]). At 200 K the O 2p band nearly restores its initial intensity showing that water desorption is almost complete. All spectra obtained at 200 K and above reveal small Ce^{3+} resonant peaks which are however similar to that of the clean surface at 120 K.

In order to investigate the thermal evolution of Ce^{3+}/Ce^{4+} concentration ratio we plotted the corresponding RERs in Fig. 4, together with RERs obtained for nonwater exposed stoichiometric surface and water-exposed reduced surface. The points at 120 K, marked by a rectangle, were obtained for non-exposed surfaces. RER of the stoichiometric CeO_2 surface after water adsorption at low temperature exhibits a maximum at $T = 170$ K indicating an increase of the Ce^{3+} state concentration followed by a subsequent decrease at higher temperatures. It indicates that water adsorption/desorption process induces limited temporary formation of the Ce^{3+} centers. Thus the above mentioned appearance of the Ce^{3+} intensity due to the cooling of the non-exposed surface can also be explained in terms of the water–ceria interaction because the cold sample adsorbs the residual background water which remains in the chamber after repeated water adsorption experiments. In Fig. 4 we also plotted the reference RER curve for CeO_2 sample not exposed to water. Very low value of RERs within the whole

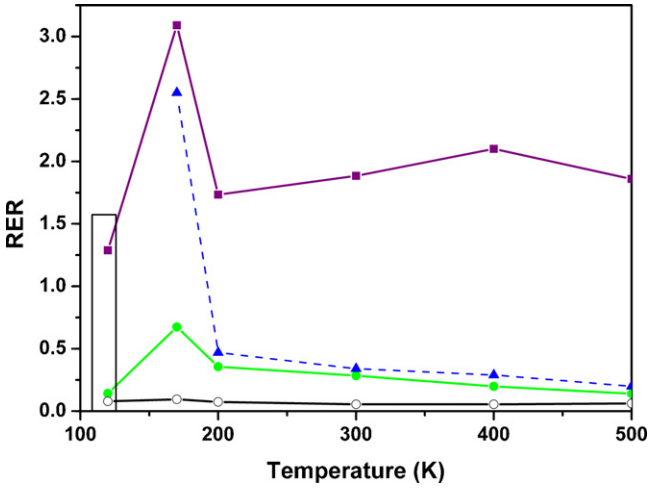

Fig. 4. RER curves obtained upon water adsorption and annealing: CeO_2(1 1 1) (●); CeO_{2-x}(111) (■); CeO_{2-x}(1 1 1) for the 2.3 eV component (▲). RER curve marked by (○) was measured on clean CeO_2(1 1 1). The points at 120 K, marked by a rectangle, were obtained for non-exposed surfaces.

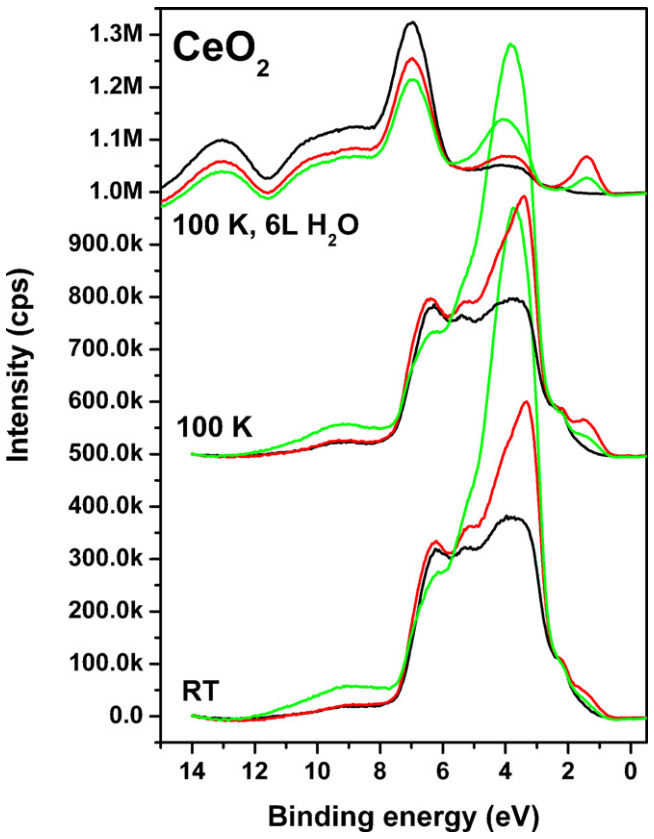

Fig. 5. On- and off-resonance valence band spectra taken at PE = 124.8, 121.4 and 115 eV for stoichiometric CeO_2(1 1 1) surface at room temperature (RT) and 100 K and 6 L of water adsorption at 100 K.

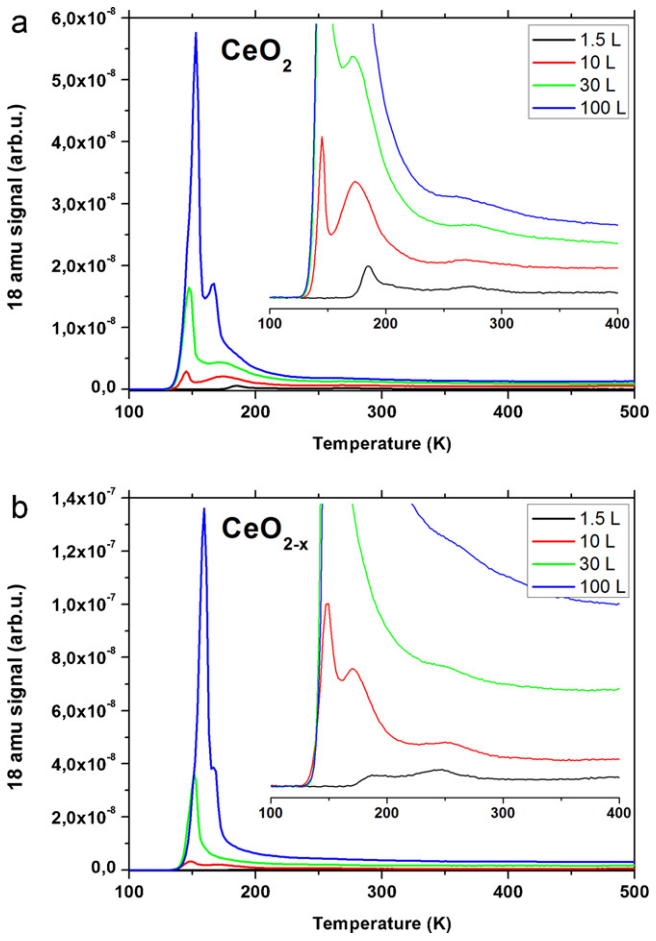

Fig. 6. Series of thermal desorption spectra acquired after various exposures (1.5 L, 10 L, 30 L, and 100 L) with water at 100 K on (a) stoichiometric CeO_2/Cu(1 1 1) surface and (b) CeO_{2-x}/Cu(1 1 1) partially reduced surface. The heating was linear with the rate of 2 K/s.

temperature range clearly shows that the Ce^{3+} state formation is not a thermal effect.

Water interaction with cerium oxide surface at low temperature was further examined by exposing the CeO_2 sample to 6 L of water at 100 K. This amount of H_2O was sufficiently low not to obscure the VB signal from ceria at this low temperature. The results presented in Fig. 5 confirm that water is reducing the surface even at 100 K. The VB spectra exhibit mixed character of cerium oxide and adsorbed molecular water.

Results of TPD experiment performed following 100 L water exposure of CeO_2 at 100 K are shown in Fig. 6a. Desorption of water is observed between 130 and 200 K which confirms that water is adsorbed in a molecular state at 120 K on the CeO_2 surface. This is also in agreement with the findings in Refs. [7,10]. Additionally, thermal desorption spectra were acquired after smaller exposures (1.5 L, 10 L, 30 L) in order to better resolve various adsorption states at the surface. The lowest temperature desorption peak with maximum in the range of 145–155 K originates from the water multilayer, while the single water layer leaves the surface around 170–185 K. The broad feature around 275 K has been attributed to a recombinative desorption of hydroxyl species with surface hydrogen, in accord to our PES observations.

Analysis of the STM images (see Section 3.1) together with corresponding RERs of the CeO_2 sample which were subject to the same experimental procedure revealed that the surface did not undergo any morphological or RER changes that could be associated with formation of oxygen vacancies or any other low coordination sites. Thus, we associate the immediate formation of Ce^{3+} centers upon water adsorption on ceria with a purely electronic water–oxide interaction effect that will be discussed below.

In Fig. 7a we present XPS O 1s spectra obtained with Al Kα X-ray source excitation. The spectrum taken from the clean CeO_2 sample at 120 K exhibits single peak at 529.5 eV which corresponds to the cerium oxide lattice oxygen, O_L [29,30]. The spectrum obtained after multilayer water adsorption shows a single peak at 534.0 eV which is typical for molecular water [3,4,6,7]. Subsequent annealing to 170 K gives two states (water and ceria), indicating that water was still molecular, and a new state which appears at BE = 531.5 eV, corresponding to formation of hydroxyl groups OH [3,4,6,7]. In Fig. 7b we plotted concentration ratios of H_2O, OH, and O_L relative to the total amount of detected oxygen O 1s. The amounts of the particular oxygen species were obtained by fitting the oxygen spectra using Gaussian shapes of peaks. In agreement with the TPD experiment (Fig. 6a) vast majority of water desorbs below 200 K however small amounts of water and hydroxyls (OH) still remain at the surface even at 500 K. Therefore a relative decrease of the RER above 170 K can be associated with water desorption and, eventually, with OH formation. According to Refs. [7,9,10] water dissociation occurs at oxygen vacancies, or in general at surface defects, so in the case of stoichiometric ceria we can expect that OH groups are located at CeO_2(1 1 1) terrace boundaries, see Fig. 1.

With the aim to better elucidate the role of the oxygen vacancy in the water–ceria interaction mechanism we performed the same experiment as described above with the reduced cerium oxide sample prepared by ion irradiation (cf. Fig. 1b). The on-resonance and off-resonance spectra obtained upon water adsorption and annealing of the CeO_{2-x} sample are presented in Fig. 8a, together with the

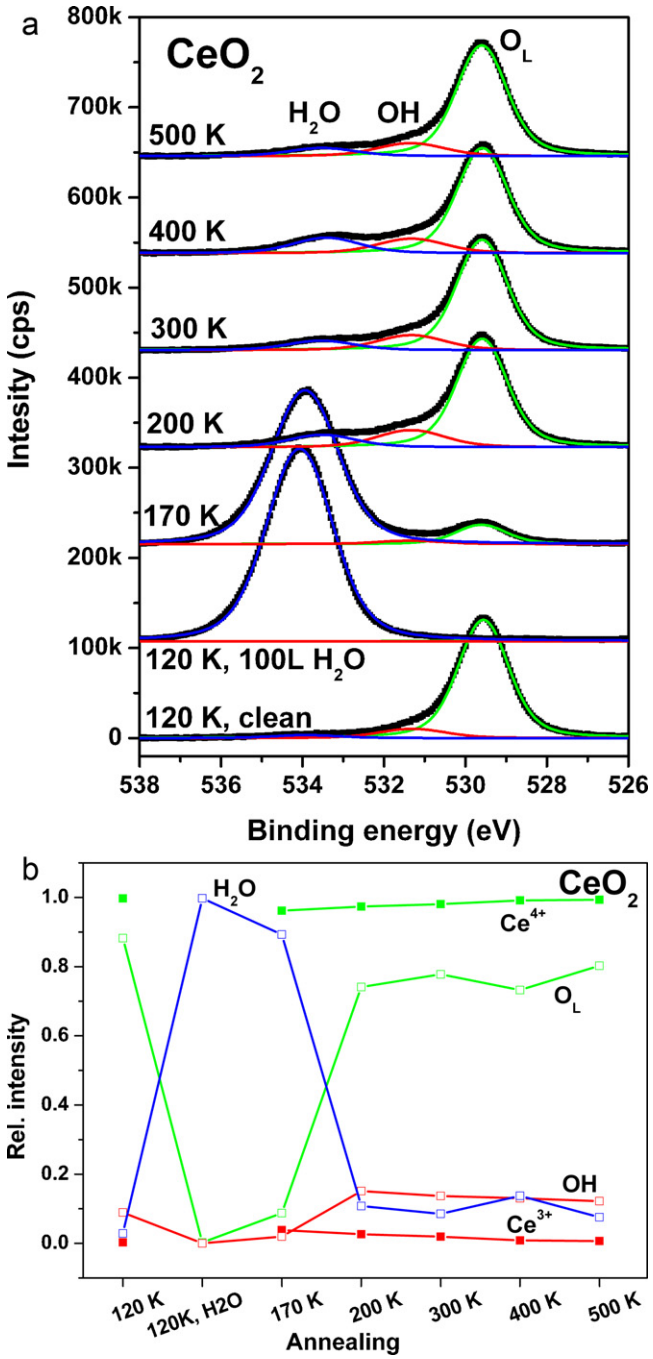

Fig. 7. (a) O 1s XPS spectra, PE = 1486.6 eV, of non-exposed CeO_2(1 1 1) surface and water adsorbed at 120 K and annealed as indicated. (b) Variation of O 1s concentration ratios for water (H_2O), hydroxyl (OH), and lattice oxygen (O_L) and Ce 3d concentration ratios for Ce^{3+} and Ce^{4+} in the case of the stoichiometric CeO_2(1 1 1) upon water adsorption and consequent annealing.

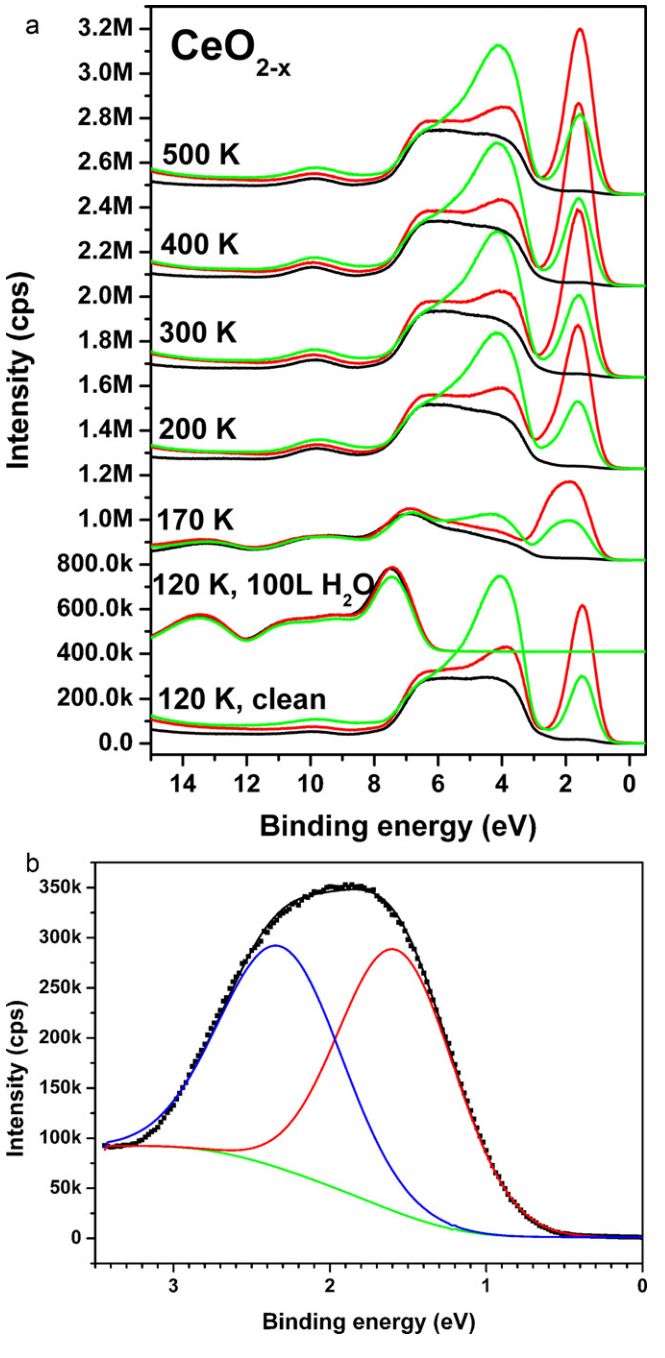

Fig. 8. (a) On- and off-resonance valence band spectra for CeO_{2-x}(1 1 1) upon water adsorption and annealing. (b) Decomposition of the Ce^{3+} resonant peak from (a) into two resonant states (170 K).

spectra of the clean sample. The clean sample spectra were taken at 120 K. Multilayer water adsorption at 120 K yield molecular water spectrum as in the case of the CeO_2 sample, in agreement with the TPD observation showing an onset of water desorption above 130 K (Fig. 6b). Corresponding RERs are plotted in Fig. 4. It reveals a strong RER enhancement at 170 K, i.e. at the same temperature as in the case of stoichiometric CeO_2. Detailed inspection of the Ce^{3+} resonance spectra taken at 170 K showed unusual broadening of the Ce^{3+} peak. A detailed look at this peak (see Fig. 8b) discloses an appearance of a new resonant feature at higher BE of 2.3 eV. The regular lower energy component has exactly the same shape and position as that of the non-exposed sample. Both peaks can be fitted with Gaussian shape. The high energy feature is distinctive only at 170 K while its contribution at higher temperatures decreases. It can be seen from Fig. 4 where variations of RERs determined for the components at 2.3 eV was added to the total RER curve, determined from the resonant peak heights.

In Fig. 9a corresponding O 1s XPS spectra are shown. Their analysis is similar to those of the above stoichiometric ceria, however both cases are quantitatively different. The relative amounts of water, OH, and O_L are plotted in Fig. 9b. In the temperature interval of 120–170 K we see again water and lattice cerium oxide O 1s peaks. At 170 K O 1s spectrum discloses noticeable co-adsorption of water and hydroxyls. For higher temperatures water nearly com-

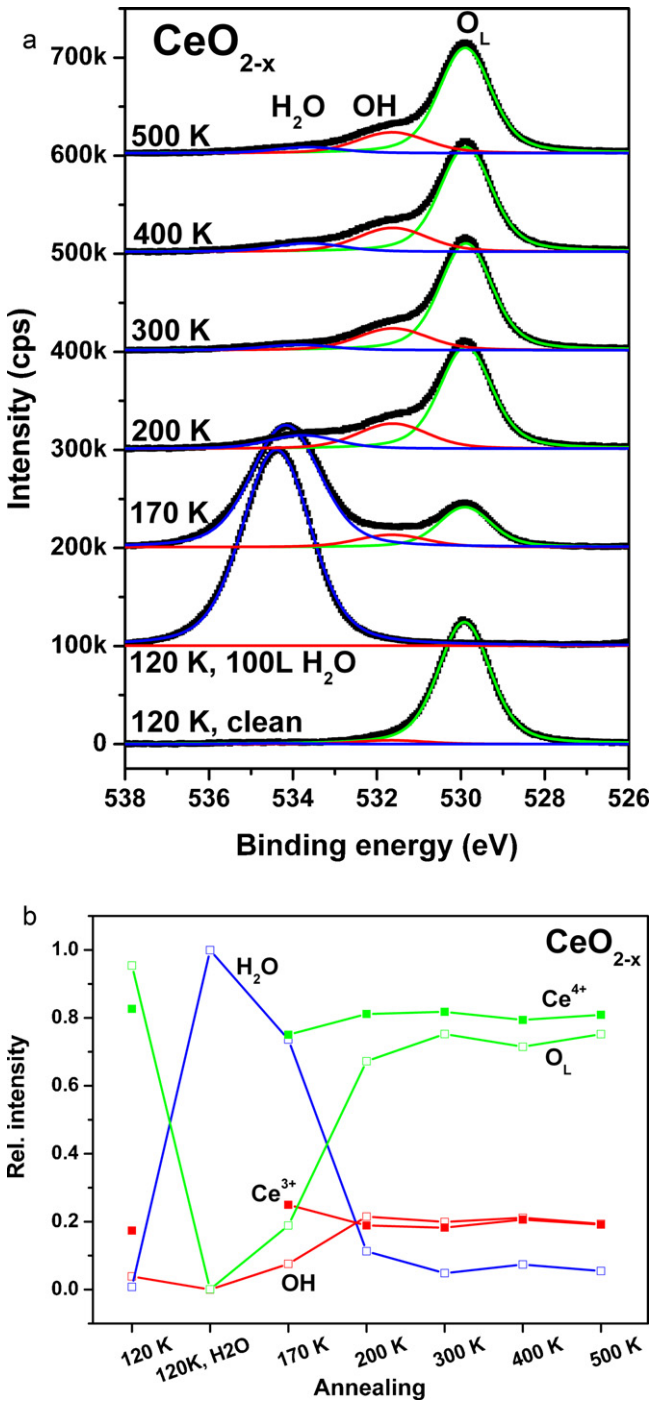

Fig. 9. (a) O 1s XPS spectra, PE = 1486.6 eV, of non-exposed CeO_{2-x}(1 1 1) surface and water adsorbed at 120 K and annealed as indicated. (b) Variation of O 1s concentration ratios for water (H_2O), hydroxyl (OH) and lattice oxygen (O_L) and variation of Ce 3d concentration ratios for Ce^{3+} and Ce^{4+} in the case of the reduced CeO_{2-x}(1 1 1) upon water adsorption and annealing.

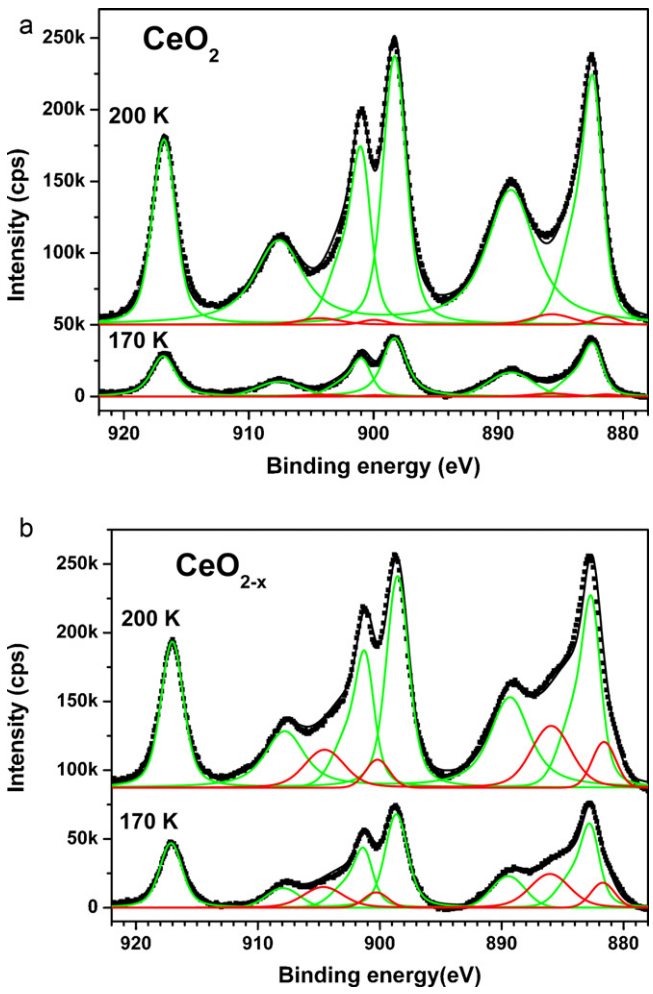

Fig. 10. (a) Ce 3d XPS spectra, PE = 1486.6 eV: CeO_2(1 1 1) after water adsorption and annealing at 170 K and 200 K. Ce^{4+} states (green), Ce^{3+} states (red). (b) Ce 3d XPS spectra, PE = 1486.6 eV: CeO_{2-x}(1 1 1) after water adsorption and annealing at 170 K and 200 K. Ce^{4+} states (green), Ce^{3+} states (red). (For interpretation of the references to color in this figure legend, the reader is referred to the web version of the article.)

pletely desorbs. The main difference as compared to the previous case is a relatively high concentration of hydroxyls due to water dissociation on oxygen vacancies, in accord to [7,9,10] as well as to our TPD data where the most strongly bound species (desorption maximum in the 250–275 K region) attributed to water produced by recombination of OH radicals with surface hydrogen are more abundant on the reduced ceria surface (Fig. 6b) than on the stoichiometric one (Fig. 6a) at the expense of the molecularly adsorbed water (compare the corresponding spectra for the same exposures on both surfaces). By comparing RER dependence on temperature plotted in Fig. 4 with O 1s intensities in Fig. 9a it seems likely that high RER value at 170 K and its decrease upon subsequent annealing at 200 K correspond to substantial decrease of water species concentration in this temperature interval. Increasing temperature above 200 K does not lead to any further changes in RER.

Variation of cerium oxide oxidation state can also be followed by analyzing Ce 3d spectra, see e.g. [18,24]. In Fig. 10a and b we present XPS Ce 3d spectra for CeO_2 and CeO_{2-x} samples taken after water adsorption and annealing to 170 and 200 K. Decomposition of the spectra to Ce^{4+} and Ce^{3+} doublets confirms the RPES results. In Figs. 7b and 9b Ce^{3+}/Ce 3d and Ce^{4+}/Ce 3d concentration ratios were plotted (here Ce 3d stands for total Ce 3d spectrum area) together with those of oxygen species. By comparing Fig. 9a and b one can clearly see that the more intense signal from OH groups in the case of the reduced sample is accompanied by an increase of the Ce^{3+}/Ce 3d ratio. Relative concentration of both OH and Ce^{3+} species at $T \geq 200$ K is equal to 0.2.

4. Discussion

Observed high Ce^{3+}/Ce^{4+} ratio upon water adsorption on cerium oxide (1 1 1) surface below 200 K where (based on our PES and STM

observations) oxygen vacancy formation can be excluded is the most important experimental result of this work. We should note that it cannot be simply explained on the basis of dissociation of adsorbed water molecules to hydrogen and OH anions because the dissociation of the O–H bond of the water molecule followed by formation of hydroxyl (H^+ bonded to lattice oxygen) and OH^- groups bonded to Ce cation is a pure acid–base reaction without any change of the oxidation state of cerium. OH fills oxygen vacancy (V_O) and hydrogen atom bonds to neighboring surface oxygen resulting in two H atoms bonded to oxygen terminated surface [9]. However, the substantial increase of RER as well as an appearance of the Ce^{3+} states in the Ce 3d and RPES spectra clearly indicates charge transfer to ceria cations and $Ce^{4+} \rightarrow Ce^{3+}$ transition. Both valence band spectra and TPD show that at 170 K the surface is covered with a thin residual layer of molecular water remaining on the surface after multilayer water adsorption. O 1s spectra gives us an evidence that at this temperature water is co-adsorbed with OH groups. Water dissociation was more pronounced on the surface reduced by ion sputtering known to create oxygen vacancies. This finding was in agreement with the results previously reported in [7,10] where the authors showed that on CeO_2(1 1 1)/Ru(0 0 0 1) surface water dissociates at oxygen vacancy sites. OH groups remained on the surface up to 500 K which was the highest annealing temperature used in this study. Senanayake et al. [10] and Fronzi et al. [9] proposed the following relationship for water dissociation on the Ce^{3+}/Ce^{4+} surface:

$$H_2O + (O_L + V_O) \rightarrow 2OH_{ads} \quad (1)$$

where V_O is an oxygen vacancy and O_L stands for adjacent surface lattice oxygen. Concentration of OH groups on the surface is proportional to the amount of Ce^{3+} present therein. The same mechanism was also proposed in [6] for water adsorption on defective TiO_2(1 1 0). In the study [6] water adsorbed dissociatively on defects at first and formed OH–H_2O complexes during further water adsorption. OH–H_2O bonding was found to be relatively weak resulting in water desorption at 170 K. On non-defective surface water adsorbed nondissociatively.

RER curves in Fig. 4 shows that both samples CeO_2 and CeO_{2-x} with different concentration of vacancies (see first values in Fig. 4) reveal increase of the RER in the temperature interval 170–400 K with a maximum at 170 K. It should be noted that RER values at 170 K can be influenced by adsorption of water and its fragments on stoichiometric and defective ceria surface. Figs. 3, 8a and 10a and b show that RPES and Ce 3d spectra are attenuated due to water adsorption at 170 K. At the same time, Ce^{3+} signal remains considerably higher than Ce^{4+} signal, which results in high RER values. This can be caused by a real increase of the Ce^{3+} concentration, or, eventually, by a more effective screening of the Ce^{4+} photoemission signal by water overlayer compared to the Ce^{3+} signal. However, small water exposures that do not cause so efficient screening of the RPES signal still do absolute increase of the Ce^{3+} intensity both at 100 K (Fig. 5) and at 200 K and higher temperatures (Fig. 3). Therefore, we can conclude that ceria reduction by water is a real effect.

The process of water adsorption on solid surfaces is not fully understood yet and therefore to render the exact mechanism of the charge transfer from water to cerium anions, which is responsible for Ce^{3+} intensity enhancement, is not straightforward. We can, however, speculate that formation of H_2O–OH and bonding of H follow the relation:

$$2H_2O + V_O + O_L \rightarrow (O_V H–H_2O) + O_L H \quad (2)$$

(V_O, oxygen vacancy; O_L, lattice oxygen; O_V, oxygen filling the vacancy) It leads to the situation where an increase of the charge at the Ce ion due to hydrogen bonding to lattice oxygen (O_LH) is not fully compensated by the charge donation to the OH–H_2O group.

Other possible explanation, which seems to be most likely here, is based on a substantial mutual charge transfer between OH–H_2O adsorbate and ceria substrate [9]. If a charge donation from the H atom to the unoccupied Ce $4f^0$ (Ce^{4+}), leading to Ce $4f^1$ (Ce^{3+}) states, is compensated due to orbital hybridization by the Ce 5d electron donation to the $(O_V H–H_2O)^-$ cerium level occupation would change, following the transition:

$$Ce4f^0 5d^1 6s^2 \rightarrow Ce4f^1 5d^0 6s^2. \quad (3)$$

In this scenario one would observe resonant behaviour due to occupation $4f^1$ of the Ce 4f level even in the case the charge neutrality is conserved. In addition, the resonant f^0 satellite, which is the final state where the screening occurs in the $5d^1 6s^2$ band in the case of simple formation of oxygen vacancies [31], would be screened less effectively with 6s electrons only. We should note that in this case the less efficient screening would lead to the new f^0 final state shifted to higher binding energy in the valence band spectrum. This mechanism provides an explanation for the appearance of the new resonant f^0 state at 2.3 eV (see Fig. 8, 170 K). However, further ab-initio calculations are necessary to support this hypothesis.

5. Conclusion

At low temperature (below 120 K) water adsorbs molecularly on stoichiometric CeO_2(1 1 1) surface while on a surface reduced by ion bombardment the adsorption is partially dissociative with formation of OH groups, preferentially bond to oxygen vacancy sites.

The surface of the ceria layer comprises oriented CeO_2(1 1 1) terraces separated by monolayer-high steps. Morphology of the CeO_{2-x} surface reduced by an ion sputtering exhibits disintegration into small islands with a characteristic diameter less than 5 nm. Water adsorption at 120 K on such surface leads to water multilayer formation which is mixed with hydroxyls. Upon annealing molecular water desorbs which is accompanied by Ce^{3+} intensity enhancement showing increase of the Ce 4f level occupancy. We propose that this behaviour indicating ceria reduction can be explained by an electronic effect of the Ce 4f charge accumulation together with Ce 5d charge depletion.

Acknowledgements

This work is a part of the research programs LC06058 and LA08022 that are financed by the Ministry of Education of the Czech Republic and 204/11/1183 financed by the Czech Grant Agency. F.D. and M.V. acknowledge the support of the 202/09/H041 Czech Grant Agency and GAUK 92209 Charles University projects.

References

[1] M.A. Henderson, Surface Science Reports 46 (2002) 5.
[2] B. Winter, R. Weber, W. Widdra, M. Dittmar, M. Faubel, I.V. Hertel, Journal of Physical Chemistry A 108 (2004) 2625.
[3] K. Andersson, A. Gomez, C. Glover, D. Nordlund, H. Ostrom, T. Schiros, O. Takahashi, H. Ogasawara, L.G.M. Pettersson, A. Nilsson, Surface Science 585 (2005) L183.
[4] T. Schiros, K.J. Andersson, L.G.M. Pettersson, A. Nilsson, H. Ogasawara, Journal of Electron Spectroscopy and Related Phenomena 177 (2010) 85.
[5] T. Schiros, H. Ogasawara, L.A. Naslund, K.J. Andersson, J. Ren, S. Meng, G.S. Karlberg, M. Odelius, A. Nilsson, L.G.M. Pettersson, Journal of Physical Chemistry C 114 (2010) 10240.
[6] S. Yamamoto, H. Bluhm, K. Andersson, G. Ketteler, H. Ogasawara, M. Salmeron, A. Nilsson, Journal of Physics: Condensed Matter 20 (2008) 184025.
[7] L. Kundakovic, D.R. Mullins, S.H. Overbury, Surface Science 457 (2000) 51.
[8] M.B. Watkins, A.S. Foster, A.L. Shluger, Journal of Physical Chemistry C 111 (2007) 15337.
[9] M. Fronzi, S. Piccinin, B. Delley, E. Traversa, C. Stampfl, Physical Chemistry Chemical Physics 11 (2009) 9188.
[10] S.D. Senanayake, D. Stacchiola, J. Evans, M. Estrella, L. Barrio, M. Perez, J. Hrbek, J.A. Rodriguez, Journal of Catalysis 271 (2010) 392.

[11] V. Matolin, J. Libra, I. Matolinova, V. Nehasil, L. Sedlacek, F. Sutara, Applied Surface Science 254 (2007) 153.
[12] F. Sutara, M. Cabala, L. Sedlacek, T. Skala, M. Skoda, V. Matolin, K.C. Prince, V. Chab, Thin Solid Films 516 (2008) 6120.
[13] T. Staudt, Y. Lykhach, L. Hammer, M.A. Schneider, V. Matolin, J. Libuda, Surface Science 603 (2009) 3382.
[14] J.A. Rodriguez, J. Graciani, J. Evans, J.B. Park, F. Yang, D. Stacchiola, S.D. Senanayake, S.G. Ma, M. Perez, P. Liu, J.F. Sanz, J. Hrbek, Angewandte Chemie-International Edition 48 (2009) 8047.
[15] J.A. Rodriguez, J. Hrbek, Surface Science 604 (2010) 241.
[16] A. Siokou, R.M. Nix, Journal of Physical Chemistry B 103 (1999) 6984.
[17] R. Wrobel, Y. Suchorski, S. Becker, H. Weiss, Surface Science 602 (2008) 436.
[18] V. Matolin, J. Libra, M. Skoda, N. Tsud, K.C. Prince, T. Skala, Surface Science 603 (2009) 1087.
[19] T. Staudt, Y. Lykhach, N. Tsud, T. Skala, K.C. Prince, V. Matolin, J. Libuda, Journal of Catalysis 275 (2010) 181.
[20] Y. Lykhach, T. Staudt, M.P.A. Lorenz, R. Streber, A. Bayer, H.P. Steinruck, J. Libuda, ChemPhysChem 11 (2010) 1496.
[21] T. Skala, F. Sutara, M. Skoda, K.C. Prince, V. Matolin, Journal of Physics: Condensed Matter 21 (2009) 055005.
[22] M. Skoda, M. Cabala, I. Matolinova, K.C. Prince, T. Skala, F. Sutara, K. Veltruska, V. Matolin, Journal of Chemical Physics 130 (2009) 034703.
[23] F. Dvorak, O. Stetsovych, M. Steger, E. Cherradi, I. Matolinova, N. Tsud, M. Skoda, T. Skala, J. Myslivecek, V. Matolin, Journal of Physical Chemistry C 115 (2011) 7496.
[24] V. Matolin, M. Cabala, V. Chab, I. Matolinova, K.C. Prince, M. Skoda, F. Sutara, T. Skala, K. Veltruska, Surface and Interface Analysis 40 (2008) 225.
[25] M. Matsumoto, K. Soda, K. Ichikawa, S. Tanaka, Y. Taguchi, K. Jouda, O. Aita, Y. Tezuka, S. Shin, Physical Review B 50 (1994) 11340.
[26] M. Abu Haija, S. Guimond, A. Uhl, H. Kuhlenbeck, H.J. Freund, Surface Science 600 (2006) 1040.
[27] W. Ranke, Surface Science 209 (1989) 57.
[28] S. Tanuma, C.J. Powell, D.R. Penn, Surface and Interface Analysis 21 (1994) 165.
[29] M.H. Engelhard, S. Azad, C.H.F. Peden, S. Thevuthasan, Surface Science Spectra 11 (2004) 73.
[30] M. Skoda, M. Cabala, V. Chab, K.C. Prince, L. Sedlacek, T. Skala, F. Sutara, V. Matolin, Applied Surface Science 254 (2008) 4375.
[31] S. Hufner, Photoelectron Spectroscopy: Principles and Applications, Springer, 2003.